Monthly Notices
of the
ROYAL ASTRONOMICAL SOCIETY

Mon. Not. R. Astron. Soc. **418,** 1517–1525 (2011) doi:10.1111/j.1365-2966.2011.19376.x

NERO – a post-maximum supernova radiation transport code

I. Maurer,[1⋆] A. Jerkstrand,[2,3] P. A. Mazzali,[1,4] S. Taubenberger,[1] S. Hachinger,[1] M. Kromer,[1] S. Sim[5] and W. Hillebrandt[1]

[1]*Max Planck Institut für Astrophysik, Karl-Schwarzschild-Str. 1, 85741 Garching, Germany*
[2]*Department of Astronomy, Stockholm University, Alba Nova University Centre, SE-106 91 Stockholm, Sweden*
[3]*The Oskar Klein Centre, Stockholm University, AlbaNova, SE-106 91 Stockholm, Sweden*
[4]*National Institute for Astrophysics-OAPd, Vicolo dell'Osservatorio, 5, 35122 Padova, Italy*
[5]*Research School of Astronomy and Astrophysics, Mount Stromlo Observatory, Cotter Road, Weston Creek, ACT 2611, Australia*

Accepted 2011 July 4. Received 2011 May 26; in original form 2011 May 10

ABSTRACT

The interpretation of supernova (SN) spectra is essential for deriving SN ejecta properties such as density and composition, which in turn can tell us about their progenitors and the explosion mechanism. A very large number of atomic processes are important for spectrum formation. Several tools for calculating SN spectra exist, but they mainly focus on the very early or late epochs. The intermediate phase, which requires a non-local thermodynamic equilibrium (NLTE) treatment of radiation transport has rarely been studied.

In this paper, we present a new SN radiation transport code, NERO, which can look at those epochs. All the atomic processes are treated in full NLTE, under a steady-state assumption. This is a valid approach between roughly 50 and 500 days after the explosion depending on SN type. This covers the post-maximum photospheric and the early and the intermediate nebular phase.

As a test, we compare NERO to the radiation transport code of Jerkstrand, Fransson & Kozma and to the nebular code of Mazzali et al. All three codes have been developed independently and a comparison provides a valuable opportunity to investigate their reliability. Currently, NERO is one-dimensional and can be used for predicting spectra of synthetic explosion models or for deriving SN properties by spectral modelling. To demonstrate this, we study the spectra of the 'normal' Type Ia supernova (SN Ia) 2005cf between 50 and 350 days after the explosion and identify most of the common SN Ia line features at post-maximum epochs.

Key words: line: formation – radiative transfer – supernovae: general.

1 INTRODUCTION

Supernovae (SNe) are classified by their spectra. The most common types are SNe Ia, Ib, Ic, IIb and II (e.g. Turatto, Benetti & Pastorello 2007). This classification links directly to the explosion mechanism, which can be either a thermonuclear explosion or the collapse of a massive star. The connection can be established since the progenitor and the explosion mechanism leave a unique imprint on the resulting SNe, which is reflected by their spectra.

In turn, one can learn about the properties of observed SNe by spectral analysis. The earliest attempts to interpret the spectra of SNe reach back to the very beginning of SN astronomy, when SNe I were classified as hydrogen poor and SNe II as hydrogen rich (e.g. Minkowski 1941). Since then, the interpretation of SN spectra has been steadily refined and several advanced tools to study SN spectra formation exist today (see below).

SN spectra are usually grouped into photospheric and nebular. It is not trivial to distinguish between the two phases on physical grounds since most radiation processes important during the earliest phases also play a role at late times. However, nebular phase spectra are dominated by clear forbidden-line emission features, which become dominant at about 200 days after the explosion. Although photoexcitation and photoionization processes are important at later epochs (e.g. Li & McCray 1996; de Kool et al. 1998; Jerkstrand, Fransson & Kozma 2011, also see this paper), they are absolutely dominant at earlier epochs.

Although the radiation from SNe is never in local thermodynamic equilibrium (LTE), this may be a reasonable first approximation directly after the explosion. However, shortly after maximum light at latest non-local thermodynamic equilibrium (NLTE) effects become important. Very little attention has been paid to these intermediate

⋆E-mail: maurer@mpa-garching.mpg.de

epochs so far, which require a full NLTE treatment of radiation transport.

Codes treating the early phase have for example been developed by Mazzali & Lucy (1993), Lucy (1999), Kasen, Thomas & Nugent (2006) and Kromer & Sim (2009). These early time codes rely at least partially on the LTE assumption and do not treat forbidden-line emission. For later epochs, numerical treatments have for example been developed by Axelrod (1980), Ruiz-Lapuente & Lucy (1992), Kozma & Fransson (1992, 1998), Eastman & Pinto (1993), de Kool et al. (1998), Mazzali et al. (2001) and Jerkstrand et al. (2011). In addition to those spectral codes specified for SNe, there exist others (e.g. Pauldrach et al. 1996; Hauschildt, Baron & Allard 1997; Hillier & Miller 1998; Baron & Hauschildt 2005; Dessart & Hillier 2005; Sauer, Hoffmann & Pauldrach 2006a; Dessart & Hillier 2010) which can be used for calculating SN spectra. The list presented here is a selection and is far from complete.

Here we present a new non-thermal equilibrium radiation transport (NERO) code which addresses especially the intermediate epochs at about 50–200 days after the explosion. We can also treat later epochs, as long as the gas shows no strong deviations from steady state (see Section 2).

In Section 2 we describe the new code. In Section 3 we compare NERO to the steady-state radiation transport code of Jerkstrand et al. (2011) (RTJ) and to the nebular code of Mazzali et al. (2001) (RTM). We also compare synthetic spectra obtained by using NERO on a SN Ia W7 model (Nomoto, Thielemann & Yokoi 1984) with observations of the proto-typical 'normal' SN Ia 2005cf at epochs between 50 and 350 days after the explosion. In Section 4 our results are discussed.

2 CODE DESCRIPTION

NERO is built on the assumption that the SN ejecta are in the steady state, i.e. heating, ionization and excitation are balanced by cooling, recombination and de-excitation, which is valid between roughly 50 and 500 days after the explosion (e.g. Axelrod 1980). These limits however depend strongly on the ejecta density and composition. Under this assumption, the spectral emission can be calculated at any epoch without considering the radiation history of the gas. The phase we can treat begins when the SN light curve starts to follow the decay of Ni and Co, which means that the gas is in thermal equilibrium and ends when the gas falls out of ionization equilibrium or when adiabatic cooling becomes important (e.g. Fransson & Kozma 1993; Dessart & Hillier 2005; Utrobin & Chugai 2005; De, Baron & Hauschildt 2010).

Details of each step are described below. The overall scheme is that we first calculate the energy deposition from radioactive nuclides from which we derive the non-thermal electron ionization and excitation rates. Using an initial guess for the ionization and excitation states and the temperature of the gas, we derive its new ionization and excitation states by solving the statistical equilibrium equations. From the ion fractions and occupation numbers, one can calculate the radiation field. This radiation field is transported through the SN ejecta using a ray-tracing transport scheme, from which we derive photoionization and excitation rates. The ionization and excitation states are iterated until the electron density and temperature and the radiation field have converged. A scheme of NERO is shown in Fig. 1.

Currently, NERO is one dimensional, but a three-dimensional version may be available in the future. For a one-dimensional model consisting of about 20 radial shells, one calculation takes a few minutes on a standard desktop computer, depending on the composition and density of the model and the desired resolution. All synthetic spectra obtained for this paper using NERO required a calculation time of the order of 5 min, which is excellent for a full-fledged NLTE radiation transport code. Still, we plan to parallelize and further optimize NERO in the future, to make modelling of observed SN spectra as efficient as possible.

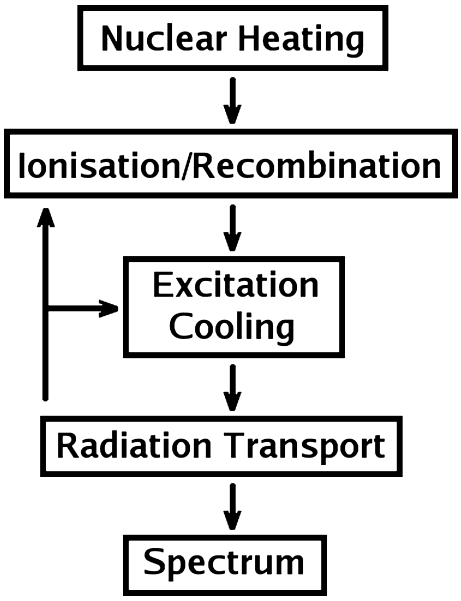

Figure 1. Code scheme of NERO.

2.1 Radioactive deposition

NERO can treat radioactive deposition by ^{56,57}Co and ^{56,57}Ni. The half-lives of these isotopes can for example be found in Seitenzahl, Taubenberger & Sim (2009). Including other radioactives would be simple. The energy deposition process is treated with a Monte Carlo approach, where Compton scattering, pair creation and photoionization are taken into account, as for example described in Milne et al. (2004) or Sim & Mazzali (2008). The accuracy of our deposition routine has been verified by comparing the energy deposition rates to calculations performed with the spectral codes of Mazzali et al. (2001) and Jerkstrand et al. (2011). Both codes use effective γ opacities, which have been shown to be a good approximation by Swartz, Sutherland & Harkness (1995). Further, we plan to compare the γ treatment of NERO to that of Sim & Mazzali (2008) and Kromer & Sim (2009) in the future, which will allow us to investigate the γ-emission spectra. From the deposited luminosity, we calculate non-thermal ionization and excitation rates as described in Maurer & Mazzali (2010) and Maurer et al. (2010a). To evaluate the non-thermal ionization rates, we estimate the fraction of the deposited luminosity causing ionization using the Bethe approximation (e.g. Axelrod 1980). The non-thermal excitation rates are calculated using the optical approximation (e.g. Axelrod 1980; Rozsnyai, Jacobs & Davis 1980). It was found by Maurer et al. (2010a) that this treatment of non-thermal ionization and excitation is accurate to at least 20 per cent for hydrogen and helium. We also compared our non-thermal electron ionization and excitation rates for various ions to rates calculated with the RTJ, which makes use of the Spencer–Fano approach of Kozma & Fransson (1992). We find overall good agreement with deviations usually of the order of 10 per cent and ∼50 per cent in the worst case. Especially, for the iron-group elements, the non-thermal rates are strongly affected by inaccurate or

poorly known atomic data and a high degree of uncertainty has to be accepted. This may be the largest source of uncertainty in all spectral calculations of SNe Ia after the maximum light.

2.2 Ionization and recombination

The ionization state of the gas is calculated under the assumption of statistical equilibrium, balancing non-thermal electron ionization, photoionization and radiative and di-electronic recombination with the charge-exchange reaction rates listed in Swartz (1994). The non-thermal electron rates are obtained as described in Section 2.1. The photoionization rates are obtained from ray-tracing radiation transport (described below) using the ground-state photoionization cross-sections from TIPTOP Base[1] (Cunto et al. 1993; Hummer et al. 1993) and a simple approximation for the lowest 40 excited states. Above the corresponding ionization thresholds, the excited-state photoionization cross-sections are assumed to be constant fractions of the ground-state cross-sections. These fractions decrease with increasing main quantum number of the excited states. All rates are corrected for stimulated recombination. We do not treat photoionization from states higher than 40 since they seem to have no noticeable influence on the spectra at the epochs of interest (50–500 d). We use the radiative and di-electronic total recombination rates of Mazzotta et al. (1998). Ground-state recombination rates are taken from Aldrovandi & Pequignot (1973) or are set to 10 per cent of the total radiative recombination rate, if not available. All the electrons recombining into excited states are distributed equally to the lowest 40 excited states from where they undergo the complete NLTE process. We plan to improve our excited-state ionization and recombination data base in the future.

2.3 Excitation

We use the line data collection of Kurucz & Bell (1995), which roughly contains 25 000 atomic levels and 500 000 lines. In principle, we can treat all elements from H to Ni and all ions from ionization states I–III (IV is taken into account for the ionization equilibrium, but does not contribute to the radiation field). However, the atomic data are poor for many ions. The atomic excitation states are calculated by solving a rate matrix (e.g. Axelrod 1980), including non-thermal electron excitation rates (see Section 2.1), photoionization and excitation rates obtained from ray-tracing radiation transport (see below) using the Sobolev approximation, spontaneous radiative de-excitation, recombination into excited states, thermal electron (de-)excitation, continuum destruction (e.g. Chugai 1987; Li & McCray 1995) and two-photon emission (TPE) of H I ($2s^1S$) and He I ($2s^{1,3}S$) (e.g. see Drake, Victor & Dalgarno 1969; Kaplan, Kleiman & Oiringel 1972 for TPE rates).

With the electron density and temperature obtained from the iteration process, we calculate collisional (de-)excitation rates. Collisional data are taken from TIPTOP and CHIANTI (Dere et al. 1997; Dere et al. 2009) data bases,[2] but also from other sources (e.g. Berrington, Fon & Kingston 1982; Hayes & Nussbaumer 1984; Berrington 1988; Mauas, Avrett & Loeser 1988; Scholz et al. 1990; Callaway 1994; Meléndez, Bautista & Badnell 2007; Bautista et al. 2009). Since our collisional data base is far from complete, we plan to regularly add and update collisional atomic data. If not available, the collision strengths are approximated (e.g. van Regemorter 1962; Axelrod 1980). However, for several hundreds of lines, there are collisional data from the literature. A serious problem at intermediate epochs, especially for treating SNe Ia, is the absence of reliable collisional data for Co.

2.4 Radiation transport

Using the ionization and excitation states obtained in the previous steps, we calculate a radiation field, which is represented by a certain amount of photon packets (typically, a few 100 000 per shell in total). These packets have the same wavelengths as the emitting lines or in the case of recombination, the wavelengths of the ionization thresholds of the recombining states. The number of photon packets representing a radiation process (emission, recombination) depends on its luminosity. More luminous radiation processes are represented by more photon packets, to increase the accuracy of the calculation.

In each radial zone, the photon packets are generated at random positions and they are sent through the SN envelope in random directions. On their way out, the photon packets propagate on straight lines and encounter bound–bound and bound–free absorption and electron scattering. To treat continuum processes, the distances to the next scattering line and to the edge of the neighbouring grid cells are calculated to obtain the continuum optical depths. After line scattering or after reaching a new grid cell, these distances are re-calculated. In contrast to classical Monte Carlo transport, no random optical depth is drawn, but the photon packets lose parts of their energy to all available continuum processes. An exception is electron scattering, which is treated by drawing a random optical depth using a classical Monte Carlo approach.

When reaching an atomic line the probability for line absorption is calculated in the Sobolev approximation. This is expected to be an excellent approximation for SN ejecta due to the large velocity gradients in their ejecta. However, the accuracy of this approximation was questioned (e.g. Baron, Hauschildt & Mezzacappa 1996), since the overlap of lines is neglected. Coming into resonance with two strong lines, closely neighboured in frequency space, a Sobolev treatment prevents photons to come into resonance with the redder of the two lines if they are absorbed in the bluer one. In reality, however, both lines would have the chance to absorb the photon if their line profiles overlap. If this effect is really significant it remains to be shown in calculations directly comparing a Sobolev treatment and a non-Sobolev treatment for realistic models since the majority of transitions with overlapping line profiles will be weak. Such a comparison was performed by Eastman & Pinto (1993) (also see Pinto & Eastman 2000), however, using a relatively small line list. They found no significant differences when using Sobolev approximation, but final conclusions are not possible yet.

While propagating, the photon packets lose parts of their energy according to the respective optical depths (or change their direction after electron scattering), and can be absorbed to 100 per cent if the optical depth is sufficiently large. This is different compared to classical Monte Carlo transport, since the energy of the photon packets is not conserved within one iteration step.

The absorbed energy is converted into excitation and ionization rates, which are used in the next iteration step to calculate the new excitation and ionization state of the ejecta. Therefore, all the absorbed energy undergoes the full NLTE process, including fluorescence, upward and downward electron collisions, photoionization, recombination, continuum destruction and TPE, and is re-emitted in new photon packets in the next iteration step, again in random directions.

[1] http://cdsweb.u-strasbg.fr/OP.htx
[2] http://www.chiantidatabase.org/

3 CODE RESULTS

3.1 Comparison to other codes

In this section, we compare NERO to the RTJ and RTM. RTJ is a steady-state radiation transport code, which is built on similar physical assumptions as NERO. While NERO treats the NLTE process completely, RTJ does not allow upward excitation of photoexcited levels. However, at least at the late epochs, which have been chosen for the code comparison, this seems to have no observable influence on the synthetic spectra (see below). RTJ has been applied to study the very late phase of SN 1987A so far (Kjær et al. 2010; Jerkstrand et al. 2011).

RTM is a nebular code based on the ideas of Axelrod (1980) and Ruiz-Lapuente & Lucy (1992), therefore, neglecting all radiation transport effects. It has widely been used in the literature (e.g. Silverman et al. 2009; Mazzali et al. 2010) to study nebular spectra of all types of SNe.

While NERO and RTJ are currently available in one-dimensional versions only, there are three-dimensional versions of RTM (Maeda et al. 2002; Maurer et al. 2010b).

A code comparison is interesting, since all three codes have been developed independently and use different numerical methods, physical assumptions and partially different atomic data.

For the comparison of RTJ and NERO, we chose the 13C model of Woosley et al. (1994). At 200 and 400 days after the explosion excellent agreement (see Figs 2 and 3) is observed. At 200 days there is some difference in the [Ca II] infrared triplet. The [Ca II] 7300 and 8500 Å features are produced in the core of the SN, where both codes predict very similar fractions of Ca II. In NERO, the 8548 Å component additionally scatters in the 8662 Å component further out in the ejecta. This does not happen in the RTJ calculation, because the Ca II fraction is ∼10 times lower (with Ca III being higher), making the 8662 Å transition optically thin. The main reason for this discrepancy is likely a radiation transport effect, since both codes use different Ca II photoionization cross-sections, which become very important for the ratio of Ca II to Ca III in the He rich, outer zones. However, this is difficult to follow in detail, since many radiation processes have influence on the radiation field and its interaction with atoms and ions. At 400 days NERO produces a [S II] feature around 4070 Å, which is not produced in RTJ, since the relevant [S II] transition is missing in the RTJ atomic data. Also, the Fe continuum around 5000 Å shows some differences. These deviations are caused by small differences of the ionization balance, electron density and temperature and the different atomic data used in the two codes. The 13C model is found to show very strong Ca II emission in both calculations, which can however be explained to be a mixing effect. In the 13C model, all the Ca is mixed with the other elements microscopically. Since Ca II has a low-excitation potential and large collision strengths, it radiates strongly, if it is mixed into large amounts of hydrogen, helium or oxygen.

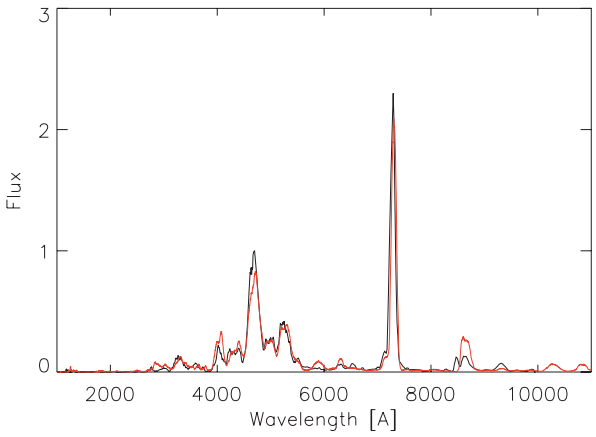

Figure 2. Synthetic spectra of the Woosley et al. (1994) 13C model at 200 days after the explosion. The RTJ calculation is shown in black, while the red curve was produced using NERO. The agreement is excellent.

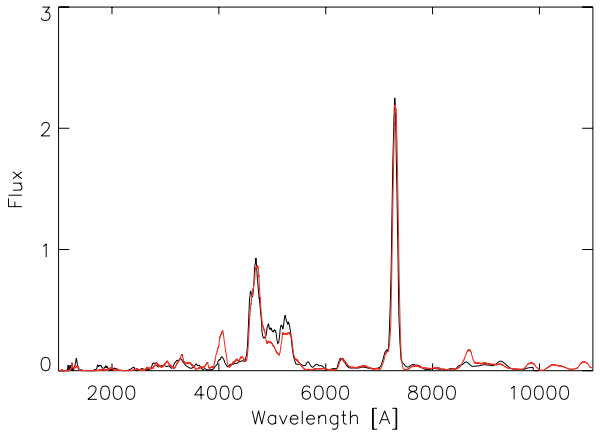

Figure 3. Synthetic spectra of the Woosley et al. (1994) 13C model at 400 days after the explosion. The RTJ calculation is shown in black, while the red curve was produced using NERO. There is some disagreement, especially in the Fe-dominated region around 5000 Å, but in general the agreement is excellent.

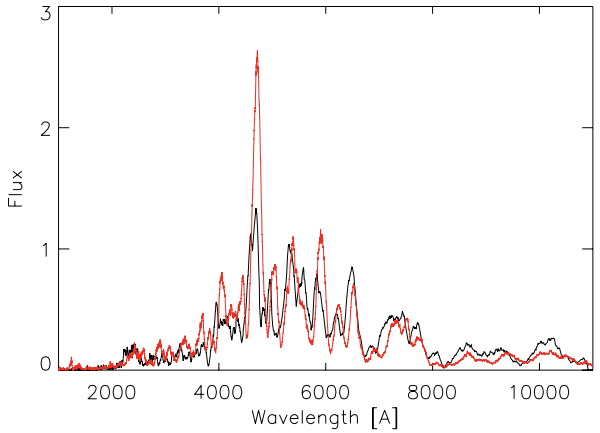

Figure 4. Synthetic spectra of the W7 model at 94 days after the explosion. The RTJ calculation is shown in black, while the red curve was produced using NERO. The agreement is reasonable, apart from a Fe III feature around 4600 Å and a Co III feature around 5900 Å.

Another comparison of NERO and RTJ was performed for a Type Ia W7 model (Nomoto et al. 1984) at 94 and 338 days after the explosion. The agreement at both epochs is good (see Figs 4 and 5). However, at 94 days after the explosion, there is a strong deviation around 4600 and 5900 Å. These features are caused by Fe III and Co III, respectively. The fraction of these ions is similar in both calculations, which means that the ion abundance cannot be a main reason for these differences. Since both features are dominated by collisional excitation from ground levels and since the electron temperature and the density are similar in both calculations, it is likely that the differing sets of atomic data used in NERO and RTJ are responsible for most of the deviation. Also, there is is an important fraction (∼15 per cent at 5000 km s^{-1}, increasing with velocity) of

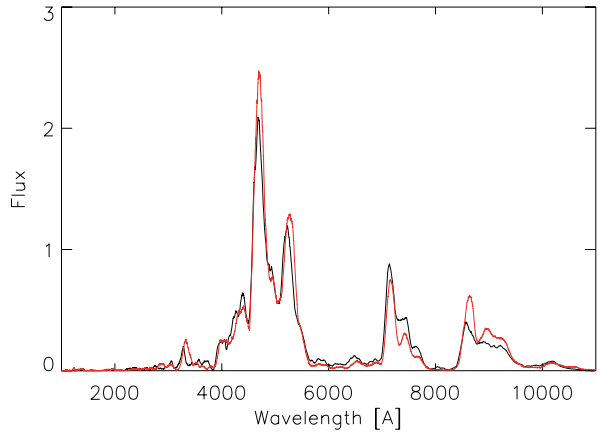

Figure 5. Synthetic spectra of the W7 model at 338 days after the explosion. The RTJ calculation is shown in black, while the red curve was produced using NERO. There is some disagreement, but in general the agreement is good.

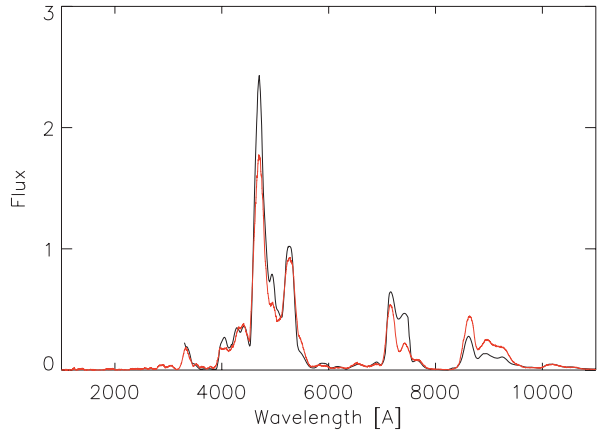

Figure 6. Synthetic spectrum of the W7 model at 338 days after the explosion. The RTM calculation is shown in black, while the red curve was produced using NERO. In general the agreement is good.

Fe IV and Co IV in the NERO calculation, which is neglected by RTJ at the moment. The recombination of these ions (and photoionization of Fe III and Co III) influences the radiation field and the cascading of ultraviolet radiation can hardly be followed in detail. It is interesting to note that the Fe III feature produced with RTJ is more consistent with observed SNe Ia spectra, while this is true for the Co III feature produced with NERO (see below).

For the comparison of RTM and NERO, we chose a Type Ia W7 model (Nomoto et al. 1984) and the 'standard' Type Ic SN 1994I (Sauer et al. 2006b). The comparison of spectra obtained with RTM and NERO for the W7 model (Nomoto et al. 1984) shows reasonable agreement (see Fig. 6). The core of the W7 model, which is observed in the nebular phase, consists of almost pure Fe (from ^{56}Ni decay). In NERO, Fe I is photoionized almost completely. The ratio of Fe II to Fe III is dominated by non-thermal electron ionization at late epochs, which is also treated by RTM. In RTM the fraction of Fe I is always set to zero. Therefore, the ionization state (and hence the electron density) of a pure Fe core obtained by NERO and RTM is similar for this model. The electron temperature of the Fe plasma obtained by NERO is about 10 per cent lower than that obtained with RTM because of the presence of excitation processes (photoexcitation, excitation by excited-state recombination, non-thermal electron excitation, more collisional transitions), which are neglected in RTM calculations.

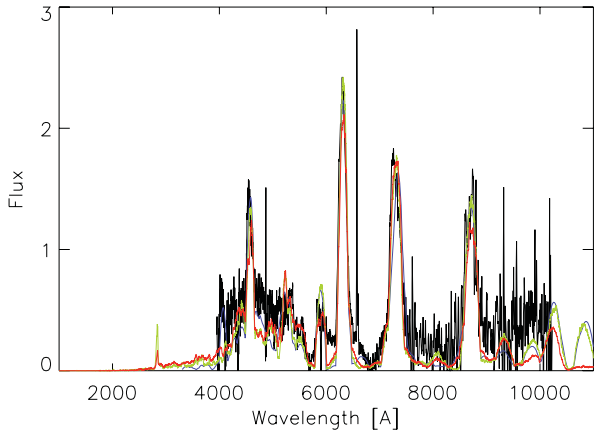

Figure 7. The spectrum of SN 1994I at about 159 days after the explosion is shown in black. The spectrum is taken from Sauer et al. (2006b) and an identification of the most important emission lines can be found there. The RTM model is shown in blue, while the NERO models 'B' and 'C' are shown in green and red, respectively. All spectra have been scaled by 2.2×10^{15} cm^2 s erg^{-1}. All models seem to fit the observed spectrum equally well. Their properties are listed in Table 1.

Since RTM has exclusively been used to derive SN core ejecta properties (and not for predicting spectra from explosion models), we also compare modelling results of RTM and NERO. For this comparison, we chose SN Ic 1994I, which has been studied in detail by Sauer et al. (2006b). They derived a total core mass ($v <$ 5500 km s^{-1}) of 0.43 M$_\odot$ and a ^{56}Ni mass of 0.07 M$_\odot$, which were also found to be consistent with the observed light curve of SN 1994I. We fit the observed spectrum with one-zone models (see Fig. 7), as it was done by Sauer et al. (2006b) [see Table 1, model 'A' (RTM) and 'B' (NERO)].

In general, the masses estimated for Na, Mg, Si, S and Ca deviate in RTM and NERO calculations. This is expected, since these elements are strongly influenced by photoionization, which is not treated in RTM. Therefore, one derives more mass for the elements which are estimated from the neutral component (e.g. Na and Mg), and less for those which are estimated from ionized states (e.g. Ca) using NERO.

Another important difference is found for the estimate of the total and the ^{56}Ni mass. These two quantities can be considered as the main properties of any SN and should be in unison with its light curve. While the RTM calculation is consistent with the light curve (see Sauer et al. 2006b), the NERO calculation seems to show too much total mass and too little ^{56}Ni (see Table 1, model 'B') to be consistent with the light curve modelling results of Sauer et al. (2006b).

This can have several reasons. Unfortunately, the intrinsic uncertainty of light curve modelling is hard to estimate and there is

Table 1. SN 1994I: (A) RTM one-zone model; (B) NERO one-zone model and (C) NERO small-scale separation model.

	C (M$_\odot$)	O (M$_\odot$)	Na (M$_\odot$)	Mg (M$_\odot$)	S (M$_\odot$)	Ca (M$_\odot$)	Ni (M$_\odot$)
A	0.09	0.2	0.0002	0.002	0.02	0.001	0.07
B	0.2	0.6	0.01	0.1	0.03	0.0004	0.03
C	0.07	0.2	0.05	0.1	0.01	0.002	0.05

always some degeneracy between ^{56}Ni and total mass, especially when radiation transport is treated in rough approximation.

However, assuming that the ^{56}Ni and total mass derived by Sauer et al. (2006b) are correct, the discrepancy of the main properties can be explained by the oversimplified input model that was used in the calculation. It is well known that mixing of the ejecta does have an important effect on the resulting spectra (also see above).

While for the code comparison of RTM and NERO a one-zone model has been used, a real SN is certainly more complex. Apart from large-scale asymmetries (which are not necessarily expected in SN 1994I), the ejecta can be structured on much smaller scales. If ^{56}Ni and other elements are separated, the ratio of Fe and other element lines changes. This, in turn, influences the estimate of the ejecta properties.

Mixing can influence the spectrum in two ways. First, separation of ^{56}Ni and other elements reduces the γ heating in the non-radioactive zones. However, in the intermediate nebular phase this effect is weak, since the γ opacity is low and positrons do not dominate yet. More importantly, when separated, carbon or oxygen rich zones cannot cool via Fe emission lines. This means that separating ^{56}Ni from other elements in the nebular phase can lead to stronger emission of those elements than with perfect mixing, which may seem counter-intuitive on a first glance.

To demonstrate this, we model SN 1994I using NERO again, this time separating Fe and O in several thin shells to simulate a separation of the ejecta on small scales. The derived ^{56}Ni and total mass change strongly (see Table 1, model 'C') and become more consistent with the light curve estimate of Sauer et al. (2006b). Of course, such an approach is highly degenerate and a broad variety of modelling results is possible.

This causes an unfortunate situation. On the one hand, detailed knowledge of the mixing of the ejecta on large and small scales is necessary to derive the main ejecta properties. On the other hand, this information is poorly constrained from observations and explosion models, especially on the small scales. Therefore, mixing poses a problem for deriving ejecta properties of stripped-envelope core-collapse SNe from modelling. Within these uncertainties, RTM seems appropriate to derive the main properties of SNe. For NERO calculations, more elaborate input models seem to be necessary to become consistent with the light curve modelling.

3.2 Comparison to observations

To further test the reliability of NERO, we calculate synthetic spectra for a W7 model (Nomoto et al. 1984), which is expected to reproduce the spectra of 'normal' SNe Ia, although this has never been tested at intermediate epochs. We compare our synthetic spectra to SN Ia 2005cf (Garavini et al. 2007; Wang et al. 2009), which can be regarded as a prototype of 'normal' SNe Ia. The calculations are performed at 47, 94 and 338 days after the explosion (see Figs 8, 9 and 11).

At 47 days after the explosion, the agreement between the synthetic and the observed spectra is acceptable, given that Co collisional data and forbidden lines are poorly known. It is interesting to note that the prominent feature at ∼8500 Å, which is usually thought to be a Ca II P-Cygni profile, could be strongly influenced by Co II emission in the observed SN Ia at this epoch. The collisional data for Co II are very poor and it is not unlikely that we underestimate (or overestimate) the Co emission in our calculation. Since important Co collisional data is missing, this remains a speculation.

At 94 days after the explosion, there is serious disagreement between the observed and synthetic NERO spectrum around 4600 Å.

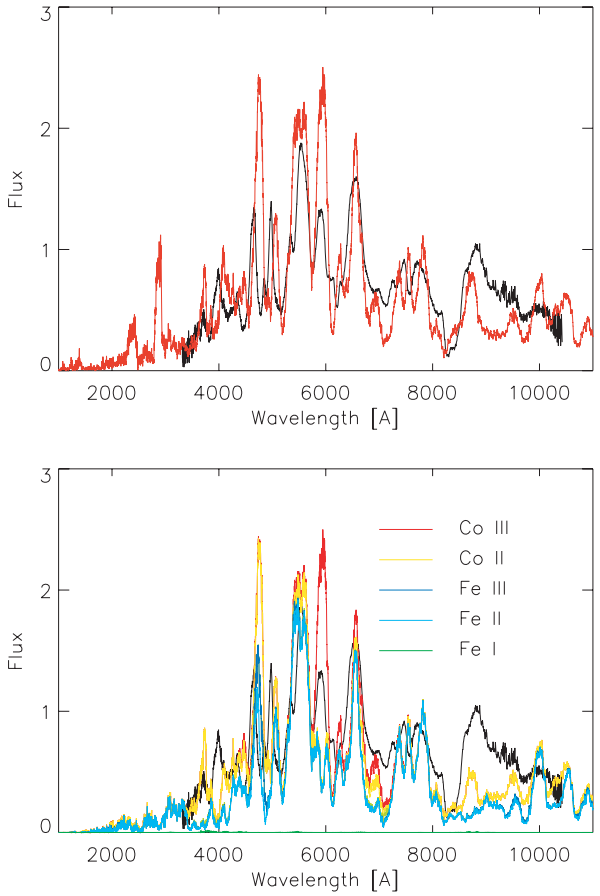

Figure 8. The spectrum of SN 2005cf at about 47 days after the explosion (Wang et al. 2009) is shown in black (upper panel) or light grey (lower panel). The spectrum was scaled by a constant. The coloured curves were produced using NERO on W7. Upper panel: the red line shows the total synthetic flux. In general the agreement is good. It is important to note that the early-time ejecta are dominated by Co II & III, which have poorly known collisional data. Lower panel: the flux of Co III (red), Co II (orange), Fe III (dark blue), Fe II (light blue) and Fe I (green) is shown separately. Please note that the flux in each line is the flux from the correspondingly coloured line to the next one below. Most features are reproduced well. Disagreement is found around 4600 Å (Fe II, Co II), ∼5900 Å (Co III) and around ∼8700 Å, which is possibly Ca II and [Co II] in the observed spectrum. Our synthetic spectra contain contributions from elements other than Fe or Co, which are not shown in the lower plot.

Interestingly, in the synthetic spectrum this feature is dominated by Fe III (see Fig. 9), while another feature, which matches the observations well, at ∼5900 Å is dominated by Co III. The RTJ spectrum of W7 (see Fig. 10) fits the 4600 Å much better, but underproduces the flux around 5900 Å. Therefore, there seems to be a problem with the ratio of the Fe III and Co III line emission in both calculations. Although, one should not expect that the W7 model can reproduce the spectra of SN 2005cf in all details, this could mean that our atomic data for Fe are inaccurate or that our approximations for example for the excited-state ionization cross-sections are too simple. In any case, the lack of reliable Co II and Co III data poses a serious problem for all SN Ia spectral calculations between maximum light and ∼150 days after the explosion before most of the Co has decayed into Fe. It has to be hoped that these data will be available in the near future.

At 338 days after the explosion the flux is dominated by Fe emission lines and the agreement of the synthetic and the

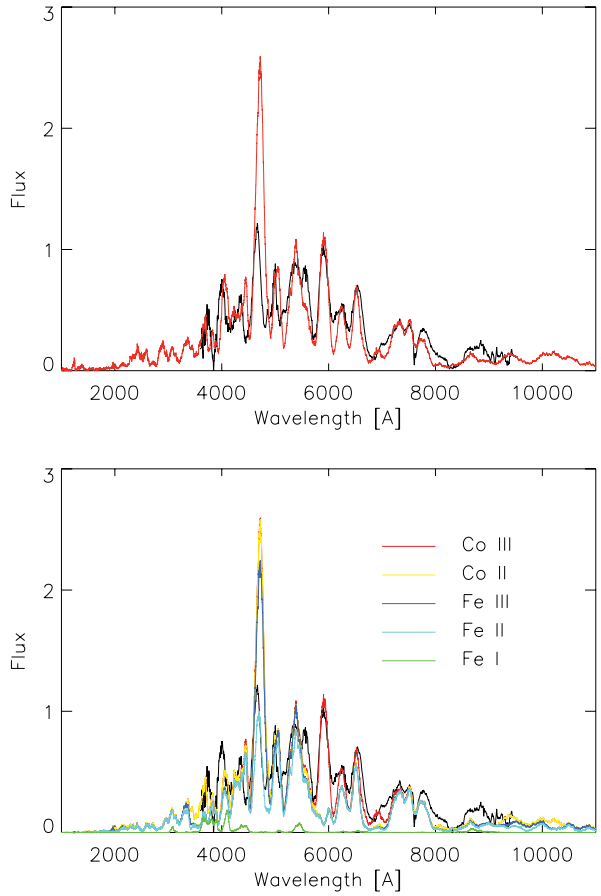

Figure 9. The spectrum of SN 2005cf at about 94 days after the explosion (Garavini et al. 2007) is shown in black (upper panel) or light grey (lower panel). The spectrum was scaled by a constant. The coloured curves were produced using NERO on W7. Upper panel: the red line shows the total synthetic flux. In general the agreement is excellent apart from the region around 4600 Å. Lower panel: the flux of Co III (red), Co II (orange), Fe III (dark blue), Fe II (light blue) and Fe I (green) is shown separately. Please note that the flux in each line is the flux from the correspondingly coloured line to the next one below. The synthetic flux exceeds the observed one at ∼4600 Å by a factor of ∼3 and is dominated by [Fe III] emission. At the same time, the [Co III] feature at ∼5900 Å matches the observed spectrum well.

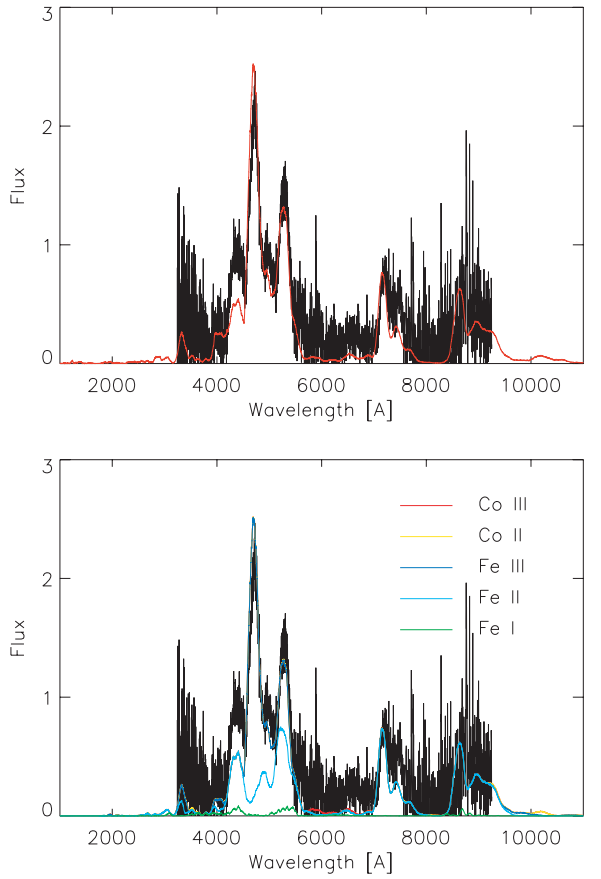

Figure 10. The spectrum of SN 2005cf at about 338 days after the explosion (Wang et al. 2009) is shown in black (upper panel) or light grey (lower panel). The spectrum was scaled by a constant. The coloured curves were produced using NERO on W7. Upper panel: the red line shows the total flux. In general the agreement is good. Lower panel: the flux of Co III (red), Co II (orange), Fe III (dark blue), Fe II (light blue) and Fe I (green) is shown separately. Please note that the flux in each line is the flux from the correspondingly coloured line to the next one below. Co features can be observed around 6000 and 10 000 Å. Their strength may be underestimated in our calculation.

observed spectrum is good. At those epochs the nebular spectra of 'normal' SNe Ia are dominated by three prominent Fe features at roughly 4400, 4700 and 5300 Å. The Fe 'trident' is shaped by the ionization state of the Fe core, which strongly depends on both the density of the core and the ratio of radioactive and stable iron. Also, mixing with light and intermediate mass elements can influence the relative abundance of Fe ions.

While the 4700 Å feature is dominated by [Fe III] emission, the 4400 Å feature is made from [Fe I] and [Fe II]. In our synthetic spectrum, this feature is underestimated and it may well be that it contains more contribution from [Fe I] in the observed SNe Ia than predicted in our simulation. It is important to note that very small fractions of Fe I (∼0.01 per cent) are sufficient to cause observable [Fe I] lines. Such small fractions of Fe I can survive even when Fe III is present, strongly depending on photoionization, recombination and possibly charge exchange processes. This makes an accurate

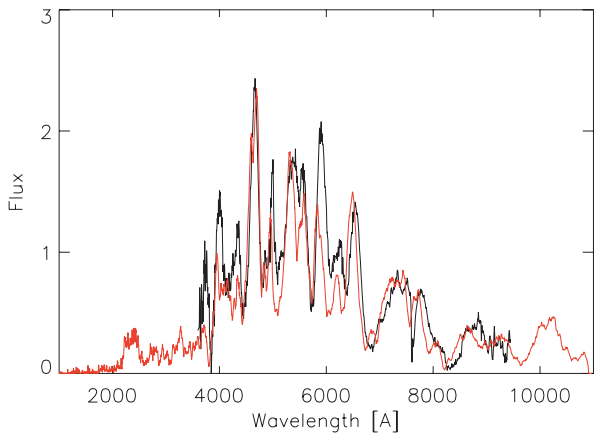

Figure 11. The spectrum of SN 2005cf at about 94 days after the explosion (Garavini et al. 2007) is shown in black. The spectrum was scaled by a constant. The red curve was produced using RTJ on W7. The reproduction of the 4600 Å feature in the RTJ calculation is much better than in the NERO calculation. Other features, for example, around 4000 and 5900 Å are reproduced better using NERO. In general, the agreement with the observation is excellent.

prediction of [Fe I] features difficult, at least at these epochs. The 5300 Å feature contains both [Fe II] and [Fe III] and shows also a [Fe I] contribution. There is almost no Co emission, except weak [Co III] lines observed around 6000 Å and [Co II] emission at about 10 000 Å. Since we have no collision strengths for Co lines from the literature, their strength may be underestimated in our simulation. The RTJ and the RTM spectra of W7 at 338 days after the explosion are similar to the NERO spectrum and are shown in the previous section.

4 DISCUSSION

A comparison to the RTJ has shown excellent agreement. This likely indicates that both codes work properly within the uncertainties of the atomic data. This is a reassuring result, since they have been developed completely independent from each other and rely on a different numerical approach.

The comparison to the RTM has also shown acceptable agreement, especially for pure Fe cores, which is important for SNe Ia. For SNe Ic, where several elements like C, O, Na, Mg, Si, S, Ca and Fe are important for the formation of the nebular spectra, we notice some differences. Most importantly, photoionization influences the mass estimated for certain elements like Na and Mg. Also, there is some disagreement regarding the main properties of the SN core (total and ^{56}Ni mass).

It is well known that mixing or a separation of the elements on small or large scales in SN ejecta can have strong influence on the resulting nebular spectra. Since this paper intends to compare codes, we do not study this effect in detail. However, it was demonstrated that the uncertainty caused by the mixing of the ejecta is comparable to the uncertainty caused by using the different codes, at least for modelling SNe Ib/c. A treatment of the mixing problem in SNe II has been presented by Kozma & Fransson (1998) and Jerkstrand et al. (2011). In 'normal' SNe Ia, this problem is less severe since the core is dominated by ^{56}Ni decay products.

By comparing synthetic Ia spectra to observations of the prototypical 'normal' SN Ia 2005cf, we have shown that the synthetic spectra produced with NERO look reasonable and are likely reliable within the uncertainties of the atomic data. Most of the observed spectral features have been identified to result from either Fe or Co emission.

At epochs between 50 and 150 days after the explosion, poorly known Co data pose severe problems for spectral modelling of SNe Ia. Atomic data are essential for calculating SN spectra. Especially for electron collisions of all kinds, the available data are often inaccurate or incomplete.

Apart from time-dependent effects, NERO treats all the radiation transport effects commonly thought to be important for the formation of SN spectra in full NLTE. Therefore, NERO calculations are especially interesting for intermediate epochs, since so far SN spectral calculations at 50–200 days after the explosion have been extremely rare. Also, the nebular phase between roughly 200 and 500 days after the explosion can be studied.

Possibly, NERO could be used to calculate (pre-)maximum spectra by imposing an estimated lower boundary flux at appropriate radii, as it is done in photospheric codes (e.g. Mazzali & Lucy 1993). With respect to purely photospheric codes, a treatment with NERO would include the effect of net emission above the lower boundary, which could then be set at lower velocities than in previous approaches. This may increase the accuracy of the (quasi-)photospheric approach considerably. We plan to investigate this possibility in the near future.

5 SUMMARY AND CONCLUSION

In this paper, we presented a new NLTE radiation transport code, which can be used to calculate synthetic spectra for all types of SNe at intermediate and late epochs.

Comparisons with the codes of Jerkstrand et al. (2011) and Mazzali et al. (2001) were carried out for explosion models 13C (Woosley et al. 1994) and W7 (Nomoto et al. 1984). The general agreement in the output of the codes is encouraging, with excellent agreement between NERO and RTJ for the 13C model, and for all codes at late times for W7.

Our treatment of intermediate epochs opens a new window for SN spectral analysis. Currently, the code is working in spherical symmetry, but a three-dimensional version may be available in the future. In its one-dimensional version, the code can be used for spectral modelling of observed SN spectra or for calculating synthetic spectra of (approximately) spherically symmetric SN explosion models.

ACKNOWLEDGMENTS

CHIANTI is a collaborative project involving George Mason University, the University of Michigan (USA) and the University of Cambridge (UK).

REFERENCES

Aldrovandi S. M. V., Pequignot D., 1973, A&A, 25, 137
Axelrod T. S., 1980, PhD thesis, California University, Santa Cruz
Baron E., Hauschildt P. H., 2005, Mem. Soc. Astron. Ital. Suppl., 7, 86
Baron E., Hauschildt P. H., Mezzacappa A., 1996, MNRAS, 278, 763
Bautista M. A., Quinet P., Palmeri P., Badnell N. R., Dunn J., Arav N., 2009, A&A, 508, 1527
Berrington K. A., 1988, J. Phys. B: Atomic Molecular Phys., 21, 1083
Berrington K. A., Fon W. C., Kingston A. E., 1982, MNRAS, 200, 347
Callaway J., 1994, Atomic Data Nuclear Data Tables, 57, 9
Chugai N. N., 1987, Astrophysics, 26, 53
Cunto W., Mendoza C., Ochsenbein F., Zeippen C.-J., 1993, A&A, 275, L5
de Kool M., Li H., McCray R., 1998, ApJ, 503, 857
De S., Baron E., Hauschildt P. H., 2010, MNRAS, 401, 2081
Dere K. P., Landi E., Young P.-R., Del Zanna G., Landini M., Mason H.-E., 2009, A&A, 498, 915
Dessart L., Hillier D. J., 2005, in Humphreys R., Stanek K., eds, ASP Conf. Ser. Vol. 332, The Fate of the Most Massive Stars. Astron. Soc. Pac., San Francisco, p. 415
Dessart L., Hillier D. J., 2010, MNRAS, 405, 2141
Drake G. W., Victor G. A., Dalgarno A., 1969, Phys. Rev., 180, 25
Eastman R. G., Pinto P. A., 1993, ApJ, 412, 731
Fransson C., Kozma C., 1993, ApJ, 408, L25
Garavini G. et al., 2007, A&A, 471, 527
Hauschildt P. H., Baron E., Allard F., 1997, ApJ, 483, 390
Hayes M. A., Nussbaumer H., 1984, A&A, 134, 193
Hillier D. J., Miller D. L., 1998, ApJ, 496, 407
Hummer D. G., Berrington K. A., Eissner W., Pradhan A. K., Saraph H. E., Tully J. A., 1993, A&A, 279, 298
Jerkstrand A., Fransson C., Kozma C., 2011, A&A, 530, A45
Kaplan S. A., Kleiman E. B., Oiringel I. M., 1972, SvA, 16, 241
Kasen D., Thomas R. C., Nugent P., 2006, ApJ, 651, 366
Kjær K., Leibundgut B., Fransson C., Jerkstrand A., Spyromilio J., 2010, A&A, 517, A51
Kozma C., Fransson C., 1992, ApJ, 390, 602
Kozma C., Fransson C., 1998, ApJ, 496, 946
Kromer M., Sim S. A., 2009, MNRAS, 398, 1809
Kurucz R., Bell B., 1995, Kurucz CD-ROM No. 23, Atomic Line Data. Smithsonian Astrophysical Observatory, Cambridge, MA, p. 23

Li H., McCray R., 1995, ApJ, 441, 821
Li H., McCray R., 1996, ApJ, 456, 370
Lucy L. B., 1999, A&A, 345, 211
Maeda K., Nakamura T., Nomoto K., Mazzali P. A., Patat F., Hachisu I., 2002, ApJ, 565, 405
Mauas P. J., Avrett E. H., Loeser R., 1988, ApJ, 330, 1008
Maurer I., Mazzali P. A., 2010, MNRAS, 408, 947
Maurer I., Mazzali P. A., Taubenberger S., Hachinger S., 2010a, MNRAS, 409, 1441
Maurer J. I. et al., 2010b, MNRAS, 402, 161
Mazzali P. A., Lucy L. B., 1993, A&A, 279, 447
Mazzali P. A., Nomoto K., Patat F., Maeda K., 2001, ApJ, 559, 1047
Mazzali P. A., Maurer I., Valenti S., Kotak R., Hunter D., 2010, MNRAS, 408, 87
Mazzotta P., Mazzitelli G., Colafrancesco S., Vittorio N., 1998, A&AS, 133, 403
Meléndez M., Bautista M. A., Badnell N. R., 2007, A&A, 469, 1203
Milne P. A. et al., 2004, ApJ, 613, 1101
Minkowski R., 1941, PASP, 53, 224
Nomoto K., Thielemann F., Yokoi K., 1984, ApJ, 286, 644
Pauldrach A. W. A., Duschinger M., Mazzali P. A., Puls J., Lennon M., Miller D. L., 1996, A&A, 312, 525
Pinto P. A., Eastman R. G., 2000, ApJ, 530, 757
Rozsnyai B. F., Jacobs V. L., Davis J., 1980, Phys. Rev. A, 21, 1798
Ruiz-Lapuente P., Lucy L. B., 1992, ApJ, 400, 127
Sauer D. N., Hoffmann T. L., Pauldrach A. W. A., 2006a, A&A, 459, 229
Sauer D. N., Mazzali P. A., Deng J., Valenti S., Nomoto K., Filippenko A. V., 2006b, MNRAS, 369, 1939
Scholz T. T., Walters H. R. J., Burke P. J., Scott M. P., 1990, MNRAS, 242, 692
Seitenzahl I. R., Taubenberger S., Sim S. A., 2009, MNRAS, 400, 531
Silverman J. M., Mazzali P., Chornock R., Filippenko A. V., Clocchiatti A., Phillips M. M., Ganeshalingam M., Foley R. J., 2009, PASP, 121, 689
Sim S. A., Mazzali P. A., 2008, MNRAS, 385, 1681
Swartz D. A., 1994, ApJ, 428, 267
Swartz D. A., Sutherland P. G., Harkness R. P., 1995, ApJ, 446, 766
Turatto M., Benetti S., Pastorello A., 2007, in Immler S., Weiler K., McCray R., eds, AIP Conf. Ser. Vol. 937, Supernova 1987A: 20 Years After: Supernovae and Gamma-ray Bursters. Am. Inst. Phys., New York, p. 187
Utrobin V. P., Chugai N. N., 2005, A&A, 441, 271
van Regemorter H., 1962, ApJ, 136, 906
Wang X. et al., 2009, ApJ, 697, 380
Woosley S. E., Eastman R. G., Weaver T. A., Pinto P. A., 1994, ApJ, 429, 300

This paper has been typeset from a TEX/LATEX file prepared by the author.